

Protein Localization in Silica Nanospheres Derived via Biomimetic Mineralization

By Mateus B. Cardoso, Heather R. Luckarift, Volker S. Urban, Hugh O'Neill,* and Glenn R. Johnson*

Lysozyme-templated precipitation of silica synthesized by sol-gel chemistry produces a composite material with antimicrobial properties. This study investigates the structural properties of the composite material that allow for retention of the antimicrobial activity of lysozyme. Scanning (SEM) and transmission (TEM) electron microscopy reveal that the composite has a hierarchical structure composed of quasi-spherical structures (~450 nm diameter), which are in turn composed of closely packed spherical structures of ~8–10 nm in diameter. Using small-angle neutron scattering (SANS) with contrast variation, the scattering signatures of the lysozyme and silica within the composite were separated. It was determined that the lysozyme molecules are spatially correlated in the material and form clusters with colloidal silica particles. The size of the clusters determined by SANS agrees well with the structural architecture observed by TEM. BET analysis revealed that the surface area of the composite is relatively low (4.73 m²/g). However, after removal of the protein by heating to 200 °C, the surface area is increased by ~20%. In addition to demonstrating a well organized sol-gel synthesis which generates a functional material with antimicrobial applications, the analysis and modeling approaches described herein can be used for characterizing a wide range of mesoporous and ultrastructural materials.

1. Introduction

Biological mineral composites derived from mineralization reactions generate complex defined architectures with mechanical properties that are often superior to those observed with

inorganic materials alone. As such, biomimetalization reactions are a common process in nature; marine diatoms, for example, sequester silicic acid from seawater in order to build intricate exoskeletons composed of amorphous silica.^[1] Higher plants also contain silica structures in the form of defensive spines and nodules.^[2] The reaction, known as biosilicification can be mimicked *in vitro* by utilizing synthetic peptides based on the native protein sequences, or identified from combinatorial peptide libraries.^[3,4] Silica formation is also observed in the presence of cationic proteins such as lysozyme and silicateins and non-biological cationic polymers such as spermine, spermidine, ethanolamine and polyethyleneimine.^[5–9] The silica structures formed in this manner are composite materials in which the inorganic mineral forms around the protein scaffolds that mediate the nucleation and precipitation of the insoluble material.^[10,11] The variability of morphologies derived by biomineralization reactions and the diver-

sity of inorganic oxides that can be synthesized using these techniques has become a versatile tool for nanotechnology.^[12] Subsequent studies have taken advantage of the *in vitro* reaction for facile immobilization of enzymes within a silica matrix for numerous biotechnology applications.^[7,12,13]

The extension of biomineralization to enzyme immobilization was derived from the observation that silica-precipitating species become entrapped during silica formation. This is a particularly interesting approach when silica formation is driven by lysozyme because the protein provides a dual functionality to the resulting composite material, i.e., structural rigidity and antimicrobial properties.^[7] The physical entrapment of lysozyme within an inorganic matrix may be expected to inhibit the native catalytic mechanism of lysozyme by preventing the necessary interaction with bacterial cell walls that is a pre-requisite for disruption of cell wall structures. Even after washing of the composite material, lysozyme activity is retained within silica composites following silicification, suggesting that portions of the catalytically active enzyme are embedded within the silica and probably leach from the matrix over time. However, standard imaging and spectroscopy methods will not unequivocally identify the location of lysozyme within the silica nanoparticles or discern whether active protein is located

[*] Dr. M. B. Cardoso,^[†] Dr. V. S. Urban, Dr. H. O'Neill
Center for Structural Molecular Biology
Chemical Sciences Division
Oak Ridge National Laboratory
Oak Ridge, TN 37831 (United States)
E-mail: oneillhm@ornl.gov

Dr. H. R. Luckarift, Dr. G. R. Johnson
Microbiology and Applied Biochemistry
Air Force Research Laboratory
AFRL/RXQL, Materials Science Directorate
Tyndall AFB, FL 32403 (United States)
E-mail: Glenn.Johnson@tyndall.af.mil

Dr. H. R. Luckarift,
Universal Technology Corporation
1270 N. Fairfield Road, Dayton, OH 45432 (United States)

[†] Present address: LNLS – Laboratório Nacional de Luz Síncrotron,
CEP 13083–970, Caixa Postal 6192, Campinas, SP (Brazil)

DOI: 10.1002/adfm.201000144

throughout the composite material or just within a localized zone adsorbed to the silica surface.

Small-angle neutron scattering (SANS) has been used to investigate the process of calcification by the protein ovalbumin to help elucidate the mechanism of eggshell formation and to characterize silica gels used as a media for growth of lysozyme crystals.^[14,15] Understanding how the protein molecule acts as a template, and defining its interaction with the silica matrix are both key to understanding the mineralization process of proteins as well as optimizing the reaction to immobilize biomolecules for practical applications. In this way, SANS may therefore provide insight into protein conformation, protein-protein interactions and structural morphology of the lysozyme-silica composite.^[16]

Herein, we examine the use of SANS to investigate the interaction of lysozyme with the silica matrix formed by biomimetic mineralization. The contrast matching technique^[17] was used to selectively highlight the scattering signature of silica and protein components during SANS experiments. To achieve this, the scattering length density of the solvent was matched to select a component by varying the D₂O/H₂O ratio in the sample, allowing the scattering signal from specific components to be observed.^[18] Scanning (SEM) and transmission electron microscopy (TEM) were used to investigate the morphology of the composites while BET analysis was employed to determine the surface area of the material. Based on the results of our analyses we propose a hierarchical structural model for this biomimetic composite.

2. Results

Preliminary experiments established a minimal concentration of lysozyme required for acceptable biomineralization yields and approximate protein capacity for the silica nanospheres. The rate and yield of particle formation increases linearly as the initial lysozyme concentration is increased. A concentration of 0.5 mg/mL was found to be the minimum required for visible silica formation (Figure S1). The pre-synthesized lysozyme-silica particles adsorb additional protein when incubated with lysozyme (Table 1). When the initial lysozyme concentration is high (see 1st experiment, Table 1), the silica particles appear to be saturated with lysozyme. However, regardless of the initial concentration of lysozyme, the final mass ratio of lysozyme to

silica (w/w) remains constant at ~1 suggesting that the silica particles have a finite protein binding capacity.

The biomineralization reactions effectively trapped the lysozyme and the native activity and structure of the enzyme appears to be retained after immobilization. In the silica formation reactions, ~90% of the lysozyme becomes associated with the resulting silica particles. A residual 5% (5.35 ± 0.32) remains in the reaction supernatant and a further 3.5% (3.63 ± 0.44) can be removed by mild washing. Accordingly, >99% of the protein was accounted in the reaction mass balance. The immobilized lysozyme can lyse the cell wall of the bacterial strain *Micrococcus lysodeikticus* demonstrating that its native hydrolase activity is retained. The K_m (M) for soluble and silica-encapsulated lysozyme was 5.3 × 10⁻⁴ (± 0.6 × 10⁻⁵) and 5.1 × 10⁻⁴ (± 0.7 × 10⁻⁵), respectively, with *M. lysodeikticus* as substrate; indicating that there is no significant change in substrate binding or activity of the lysozyme following silicification.

The nitrogen adsorption isotherms of the silica-lysozyme composites show typical type IV characteristics, with hysteresis indicative of a mesoporous matrix (Figure 1).^[19] The BET surface area of silica-lysozyme was calculated from the linear monolayer region of adsorption at low relative pressures (0.05–0.3 P/P₀) after degassing at 30 °C (Figure 1A) and 200 °C (Figure 1B). Heat-treatment of the composite material to 200 °C was used to remove the organic component and provide information on the relative volume occupied by the protein. Higher temperatures were avoided as it was previously demonstrated that the silica particle morphology will take on a sintered appearance upon extensive heating.^[7] Before heating, the surface area of the silica-lysozyme composite was 4.73 m²/g and the pore volume was 0.0085 cm³/g. After heat-treatment, the surface area and pore volume of the material increased significantly to 5.71 m²/g and 0.0108 cm³/g, respectively. The physical change is attributed to the removal of the lysozyme from the mesopores during heating. For unheated samples, the BJH pore size distribution shows a wide mesopore distribution between 5 and 15 nm with primary peaks at 6.5 and 12.2 nm (Figure 1C). However, the pore size distribution is dominated by mesopores with sizes larger than 20 nm. Adsorption measurements performed on silica with lysozyme-occluded pores (before heat-treatment) show little difference in isotherms but significant differences in the pore size distribution. After degassing the silica at 200 °C, (Figure 1D), pores with an average size of 3.4 nm are observed which is comparable to the dimensions of lysozyme (4.5 × 3.0 × 3.0 nm).^[20] In addition, the 20 nm pores present in the samples degassed at 30 °C are even more pronounced after removal of the protein at 200 °C.

SEM analysis revealed the size and morphology of silica-lysozyme composite synthesized in H₂O (Figure 2). Although the majority of particles formed are spherical in shape, closer examination of the micrographs also reveals the presence of ellipsoid and polyhedral structures (Figure 2A). At higher magnifications multilobed structures are evident that could be formed by aggregation of quasi-spherical particles (Figure 2B). This suggests that lysozyme-mediated mineralization initially yields quasi-spheres (indicated by the arrows in Figure 2B) that aggregate to form larger asymmetric structures. The particle size distribution was determined and an asymmetric

Table 1. Adsorption of excess protein to lysozyme-mediated silica particles

	1 st experiment	2 nd experiment	3 rd experiment
[Lysozyme] in initial silica particles (mg/mL)	11.95 ± 0.45	5.98 ± 0.20	2.05 ± 0.23
[Lysozyme] in silica after adsorption (mg/mL)	12.06 ± 1.02	6.59 ± 0.46	2.36 ± 0.33
Lysozyme adsorbed in excess (%)	-0.92	-10.2	-15.1
Total dry mass of silica (mg)	14.02 ± 1.55	6.6 ± 1.21	2.5 ± 0.31
Lysozyme/Silica (w/w)	-0.86	-1.0	-0.94

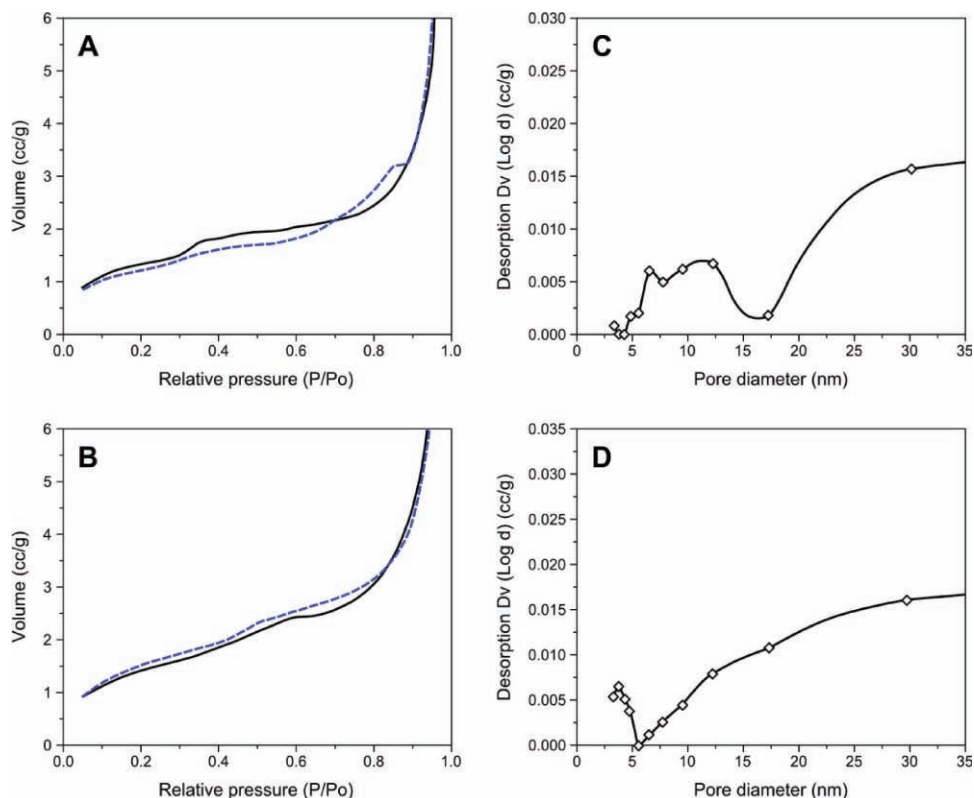


Figure 1. N₂ adsorption-desorption isotherms (A and B) and pore size distributions (C and D) of silica-lysozyme composites at 30 °C (A and C) and 200 °C (B and D).

distribution was observed with sizes ranging from 200 nm to 1 μm (Figure 2C). A Gamma distribution with particles having a diameter of 460 nm and a polydispersity index of 50% was the best fit to the data. The larger spheres present in the distribution result from the aggregation of particles similar to materials shown in Figure 2B.

Analysis by TEM shows that the structures observed by SEM are consistent with a framboid structure composed of smaller particles. The lower-magnification TEM image shows the edge

of one such structure and at higher magnification closely packed spherical particles with average diameters of 8–10 nm are evident (Figure 3A and B).

The structural properties of silica-lysozyme composites were also investigated using SANS. The contrast variation technique effectively highlighted the individual scattering contributions of the protein and silica in the composite material. The structural characteristics and morphology of the silica-lysozyme composites (presented in Figure 2) were unchanged when the samples

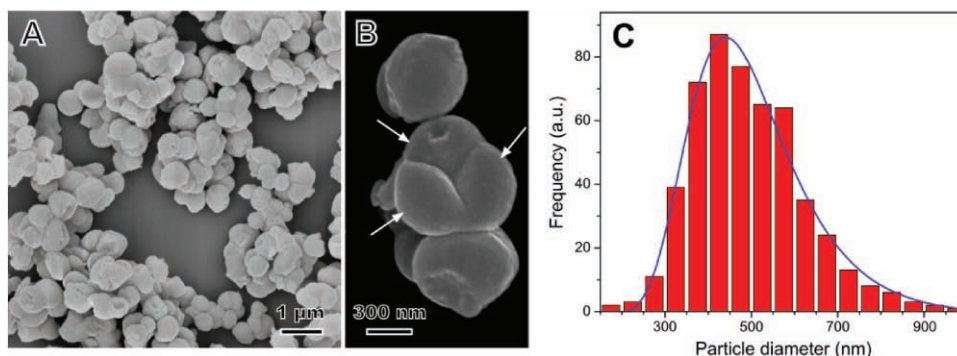


Figure 2. (A) Low and (B) high-magnification SEM images of silica-lysozyme composites. Arrows presented in image B indicates quasi-spherical particles in a possible configuration of aggregation. (C) Particle size distribution of silica-lysozyme composites (red bars) and its corresponding Gamma distribution fit (blue line).

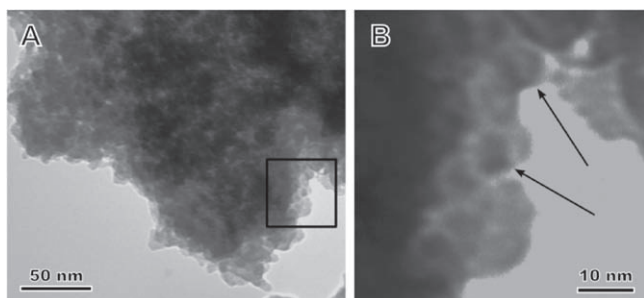


Figure 3. TEM of silica-lysozyme composite at (A) low and (B) high magnification. Inset black frame corresponds to enlarged region presented in B. The arrows indicate the presence of particles with average size dimension between 8 and 10 nm.

were equilibrated in mixtures containing different H₂O/D₂O ratios.^[21] In 42% D₂O (Figure 4), the SANS scattering profile is dominated by the scattering signature of silica because the scattering length density of the protein is the same as the solvent at this D₂O concentration.

The unified fit of the samples in 42% D₂O (shown as a full red line) helped interpret structural details in the sample on two different length scales. The fit to the low q region ($q < 1.5 \text{ nm}^{-1}$) is represented by the dotted black line. The power-law scattering exponent is -3 ($q < 0.15 \text{ nm}^{-1}$) which corresponds to the presence of either hierarchical structures or pores with rough surfaces. An accurate determination of the radius of gyration (R_g) was not possible due to the absence of a Guinier region at the low q region. However, we can estimate that such structures must have an R_g of 30 nm or larger, because a smaller R_g would influence the curve shape and diminish the quality of the fit. BET analysis supports that this structural level is related to the large pores observed in Figure 1C. The fit to the high q region ($q > 0.5 \text{ nm}^{-1}$), shown as a dashed-dotted blue line, represents the scattering contribution of

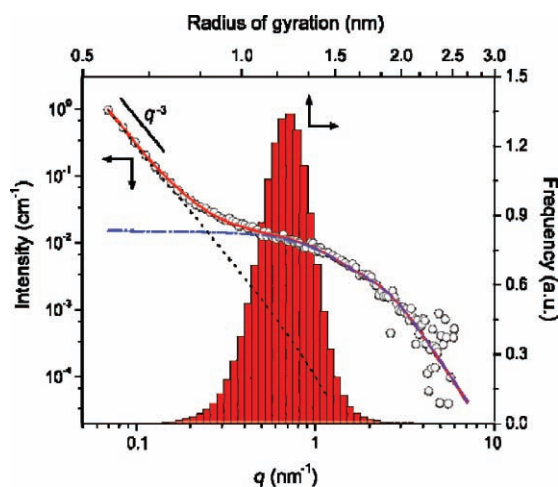


Figure 4. SANS data of silica-lysozyme composites in 42% D₂O (white circles). Unified fit is shown as a solid red line and the two fit levels are presented as dotted black line and dotted dashed blue line. Silica particle size distribution obtained from maximum entropy approach is presented.

silica particles. The R_g obtained from a Guinier fit of the shoulder, evident at $0.5 - 2 \text{ nm}^{-1}$, is 1.3 nm. The polydispersity of the silica particles was calculated using the MaxEnt procedure (Figure 4) giving a mean R_g and σ values of 1.27 and 0.14 nm, respectively.

SANS analysis of silica-lysozyme composites in 58% D₂O, the contrast match point of silica, is presented in Figure 5. As before, the unified fit (shown as a full red line) in the low q region ($q < 0.2 \text{ nm}^{-1}$) has a power law exponent of -3 , indicating that the structure or pores found at this q region has the same surface roughness and similar overall dimensions to the sample in 42% D₂O. The fit to the high q region is shown by a dashed green line and represents the scattering contribution of lysozyme. The R_g calculated from the Guinier fit is 1.8 nm which is in agreement with the values found in the literature for lysozyme in composite materials ($R_g \sim 1.7 \text{ nm}$)^[22] indicating that large aggregates of protein were not evident during the material synthesis. The presence of a peak at $q \sim 2 \text{ nm}^{-1}$ provides evidence that adjacent protein molecules are correlated in the composite material. Similar stacking signatures have been previously reported for polymer-lysozyme composites.^[22–25] In the previous studies, the position of the lysozyme correlation peak is reported to be between 1.6 and 2 nm^{-1} . The average correlation distance between two neighbor protein molecules (ζ) was calculated from the peak position using Bragg's law ($\zeta = 2\pi/\text{peak position}$) resulting in protein correlation distances between 3 and 4 nm.^[22–25] However, considering the absence of sharp Bragg peaks in the scattering pattern of Figure 5, a more accurate analysis was performed by using the correlated system method of the unified fit.^[26] The calculated ζ value is $\sim 2.1 \text{ nm}$ by this analysis which is realistic if compared to the one that could be obtained directly through Bragg's law.^[26] The degree of correlation (k) is indicative of how well the system is ordered.^[27] The upper limit ($k = 5.92$) indicates a perfect hexagonal or cubic close-packed crystal structure and k decreases to zero in an uncorrelated system.^[27] Intermediate values are indicative of less well-ordered systems. In this study, $k = 1.16$ suggests that the protein molecules are weakly correlated with each other comparable to the typical short range order of molecules in a liquid.^[28]

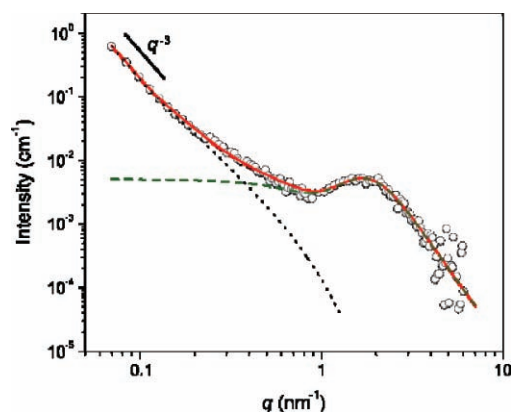


Figure 5. SANS data of silica-lysozyme composites in 58% D₂O (white circles). Unified fit is shown as a solid red and the two fit levels are presented as dotted black line and dashed green line.

SANS data of silica-lysozyme composites in 100% D₂O is shown in Figure 6A. This scattering curve represents the combined scattering contributions of the protein and silica. The unified fit is shown as a solid red line and is used to interpret the structure of the composite on three length scales. In the low q region (dotted black line) the power law exponent is -3.3 , similar to the values calculated in 42% and 58% D₂O. The peak at $q \sim 2 \text{ nm}^{-1}$ is interpreted as the correlation peak signature of lysozyme, based on the analysis of the silica gels in 58% D₂O. An R_g of 1.6 nm, $\zeta = 2.5 \text{ nm}$ and $k = 2.4$ were calculated from the fit to the experimental curve in this region (dashed green line). The small differences in these values compared to the 58% D₂O data reflect the fact that the scattering contribution of silica was contrast matched to the solvent.

At the mid q range ($0.2 < q < 1 \text{ nm}^{-1}$), there is a level of organization (dotted dashed blue line) that is not observed at the contrast match points of silica or protein. This structural organization is also observed in samples that are away from the contrast match point for silica or protein, such as those equilibrated in 0 and 8% D₂O (Figure S2). The R_g obtained from this length-scale is 3.3 nm, which is significantly larger than the R_g of silica or lysozyme. Since this structural level is absent at

the contrast match point of silica or lysozyme, it is likely that it originates from an assembly of protein molecules and colloidal silica to form clusters in the composite material. The interpretation is consistent with the volume of the components of the composite, estimated from their respective R_g values, which are 44.3, 18.5 and 323.9 nm³ for lysozyme, colloidal silica, and the cluster, respectively. Analysis of the experimental data in this region (shown as a dotted dashed violet line superimposed into the solid red unified fit line) using the MaxEnt procedure resulted in a bimodal size distribution of particles (Figure 6B). The main population, accounting for 97% of the sample, has a R_g of 3.42 nm, which is in agreement with the values obtained by unified fit, and σ of 0.66 nm indicating $\sim 20\%$ polydispersity. The other population, representing around 3% of the distribution, gave an R_g of 7.78 nm ($\sigma = 1.45 \text{ nm}$), which may be attributed either to large silica-protein aggregates or to instabilities in the scattering background subtraction.

3. Discussion

Many factors affect protein-mediated synthesis of colloidal sol-gel materials from reactive metal alkoxide monomers. The factors include, pH, temperature, concentration and molar ratio of H₂O/Si, and the nature and concentration of catalyst. In the growth phase of sol-gel formation, the nascent colloidal particles aggregate to form interconnected networks or discrete clusters. In general, SiO₂ networks derived under acidic conditions yield linear or randomly branched polymeric networks, while under base-catalyzed conditions highly branched clusters are obtained.^[29]

In the present investigation, tetramethylorthosilicate was hydrolyzed under acidic conditions at a H₂O:Si molar ratio of ~ 47 followed by polymerization at pH 8. At such high H₂O/Si ratios, the hydrolysis reaction is expected to end before the condensation reaction commences.^[30] In addition, the basic pH conditions used for the condensation reaction decreases the condensation rates and results in longer polymerization times. Previous studies have reported polymerization times greater than 100 h at a 16:1 H₂O/Si ratio.^[31] However, the addition of lysozyme to the pre-hydrolyzed sol-solution results in a rapid precipitation of silica.^[7] This occurs because the condensed silica particles have a negative surface charge and form a stable colloidal suspension until the addition of positively charged lysozyme molecules which results in the formation and rapid precipitation of the silica-protein composite. Previous reports have indicated strong adsorption of lysozyme to silica mediated by hydrophobic/hydrophilic properties and electrostatic interactions between the biomolecules and nanomaterials.^[29–33]

SANS analysis provides insight into the mechanism of formation and structure of the silica-lysozyme composite material. At the contrast match point for silica, the scattering profile shows that the protein is monodisperse ($R_g = 1.8 \text{ nm}$) and not in an aggregated state in the composite. However, the peak evident at 0.2 nm^{-1} indicates that adjacent protein molecules are weakly correlated ($k = 1.16$) with an inter-protein distance of 2.5 nm, suggesting that adjacent protein molecules have a regular short-range spatial arrangement. The structural properties of the composite at the contrast match point for protein,

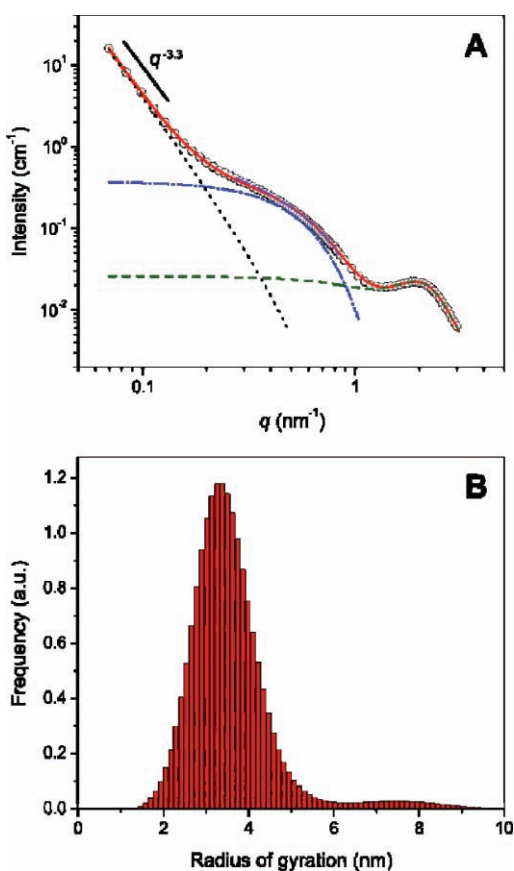


Figure 6. (A) SANS data of silica-lysozyme composites in 100% D₂O (white circles). Unified fit is shown as a solid red and the three fit levels are presented as dotted black line, dotted dashed blue line and dashed green line. (B) Particle size distribution obtained from maximum entropy approach is presented while the corresponding fit is present as a dotted dashed violet line superposed on the solid red line in panel A.

reveal an average diameter of the colloidal silica particles of 3.27 nm ($R_g = 1.27$ nm; diameter = $2\sqrt{\frac{5}{3}} R_g$) with 10% polydispersity. In addition, measurements carried out in 100% D₂O reveal the presence of an additional structural feature with diameter ~8.5 nm (R_g of 3.3 nm) which is larger than the protein and silica dimensions at the corresponding contrast match points. Since this structural feature is only visible in the SANS data measured away from the contrast match points, we propose that the composite is composed of 'fundamental' clusters ($R_g = 3.3$ nm or 8.5 nm diam.) that are formed via electrostatic interactions between silica and lysozyme. The dimension of the cluster matches well with the spherical particles observed by TEM analysis (8–10 nm).

BET analysis demonstrated that the surface area and pore size of the material increase 20 and 27% respectively after removal of the protein by heating to 200 °C. The surface area of the material is 5.72 m²/g after heating, which corresponds to a surface area of 0.06 m² for the amount of material used in this study. Accordingly, a ~3.44 m² surface area would be required to form a monolayer of 9 mg lysozyme (the amount entrapped with silica).^[34] The difference suggests that the majority of the lysozyme is present in the clusters and is consistent with the BET analysis results, which revealed the presence of a 3.4 nm pore, approximately the size of a lysozyme molecule. As described in the results section, when lower concentrations of lysozyme are used to form the composite it is possible to bind additional lysozyme to the composite indicating that there are surface sites available for lysozyme attachment. The presence of surface accessible lysozyme accounts for the observed bactericidal activity of the material.

4. Conclusions

The results of this work provide important insight into the structural organization of a biomimetic composite material composed of lysozyme and silica, synthesized through a sol-gel method. A hierarchical structure for the composite material can be proposed based on our SANS, electron microscopy, and BET analyses.

The fundamental structure in the composite is a self-assembled cluster of lysozyme molecules and colloidal silica particles schematically presented in **Figure 7A**. These clusters aggregate (**Figure 7B**) to form larger quasi-spherical structures observed by SEM (**Figure 7C**). The BET and TEM data indicates that the clusters are relatively tightly packed within the spherical structures given that the surface area and pore volumes are low compared to other mesoporous silica materials.^[32] These structures then coalesce to form the macroscopic composite material. The concomitant decrease in surface energy that accompanies the assembly of the clusters and their subsequent aggregation is the driving force for the formation of the material. We hypothesize that relatively monodisperse aggregates are formed due to size-dependent aggregation rates as suggested in the literature.^[29]

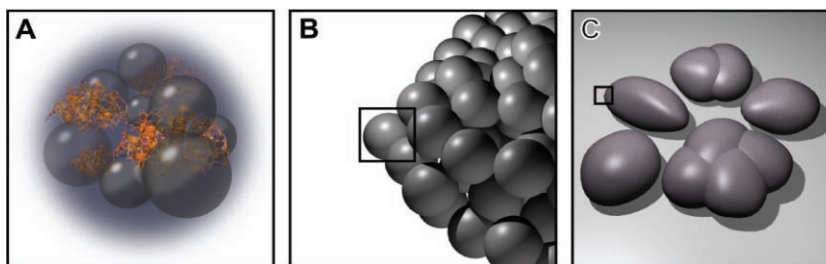


Figure 7. (A) Schematic drawing of fundamental silica-lysozyme cluster. Silica particles are shown as gray spheres while lysozyme molecules (pdb #2VBI) are presented in orange. (B) Aggregates of fundamental clusters. Black square presented in **Figure 7B** corresponds to **Figure 7A**. (C) Quasi-spherical and poly-lobular representative structures. Black square presented in **Figure 7C** corresponds to **Figure 7B**.

5. Experimental Section

Materials: Lysozyme (EC 3.2.1.17), tetramethylorthosilicate, deuterium oxide and all other chemicals were from Sigma-Aldrich (St. Louis, MO) and of the highest purity available. Silica-lysozyme composites were prepared as described previously using lysozyme as the scaffold molecule in the biomineralization process with an initial concentration of lysozyme at 10 mg/mL.^[21] Briefly, a stock solution of lysozyme (10 mg/mL) was prepared in deionized water. TMOS (1 M final concentration) was hydrolyzed in hydrochloric acid (1 mM). The precipitation mixture consisted of buffer (0.1 M phosphate, pH 8), hydrolyzed TMOS, and lysozyme, mixed at a ratio of 8:1:1. The mixture was agitated for 5 min at room temperature. The resultant particles were removed by centrifugation for 10 s and then washed twice with phosphate buffer (0.1 M, pH 8) to remove surface-associated (non-encapsulated) lysozyme.

Protein Kinetics: Protein concentrations were determined using the bicinchoninic acid (BCA) protein assay with bovine serum albumin as standard according to the manufacturer's instructions (Pierce, Rockford, IL). Lysozyme activity assays were performed with *Micrococcus lysodeikticus* cells according to the supplier's instructions (Sigma-Aldrich, St. Louis, MO).

Pore Size Distribution and N₂ Isotherms: N₂ adsorption and desorption isotherms were performed on an Autosorb-1 series instrument (Quantachrome, Boynton Beach, FL) with degassing at 30 °C and 200 °C in the relative pressure range from 0.05–0.9944 P/Po. Surface area calculations were determined from nitrogen isotherms using the BET method (0.05–0.3 P/Po) and pore volumes calculated using Barrett-Joyne-Halenda (BJH) algorithms according to the manufacturer's instructions.

Electron Microscopy: Field emission scanning electron microscopy and transmission electron microscopy (FE-SEM and TEM) were performed by Karen Kelly at the University of Florida in the Interdisciplinary Center for Biotechnology Research, Electron Microscopy Core Laboratory, Gainesville, FL. FE-SEM samples were aspirated onto graphite adhesive aluminum stubs, sputter coated 100 Å Au/Pb, and imaged with an Hitachi S-4000 FE-SEM (Hitachi High Technologies America, Inc., Pleasanton, CA). TEM samples were resuspended in water, deposited onto 400 mesh carbon-coated grids, air-dried, and examined with a Hitachi H-7000 TEM.

Small-Angle Neutron Scattering (SANS): SANS experiments were performed using the CG-3 Bio-SANS instrument at the High Flux Isotope Reactor in Oak Ridge National Laboratory.^[35] A batch of silica-lysozyme composite was prepared in phosphate buffer and samples were equilibrated in 0, 8, 42, 58, and 100% D₂O. The samples were exchanged 3 times in the respective H₂O/D₂O mixture by performing sequential centrifugation and washing steps. They were then transferred to quartz cuvettes (1 mm path length) (Hellma USA, Plainview, NY) and allowed to settle for 16 h before SANS measurements. H₂O, D₂O and an empty cell were used to determine baseline scattering. The transmission intensity

of each sample was determined before and after analysis to determine any further settling during the measurements. Buffer background and calibration measurements over the full q -range were included as control measurements. Scattering data were recorded for scattering vectors (q) $0.065 < q < 6.0 \text{ nm}^{-1}$ ($q = (4\pi/\lambda) \sin(\theta/2)$, λ is the neutron wavelength and θ is the scattering angle) using $\lambda = 6 \text{ \AA} \pm 15\%$ and a $1 \text{ m} \times 1 \text{ m}$, position sensitive He^3 -detector at sample-to-detector distances of 1.1 m and 6.8 m .

SANS data analysis was carried out using the Irena evaluation routine implemented in commercially available Igor Pro Software.^[36] A multi-level unified fit was used to describe the multiple levels of structural organization evident in the scattering data.^[37,38] In this method, the scattering provided by each structural level is the sum of a Guinier exponential-form and a structurally limited power-law tail. A generalized equation representing any number of spherical levels is written as^[37,38]:

$$I(q) = \sum_{i=1}^n G_i \exp\left(\frac{-q^2 R_{gi}^2}{3}\right) + B_i \exp\left(\frac{-q^2 R_{g(i+1)}^2}{3}\right) \left[\frac{(\text{erf}(q R_{gi}/\sqrt{6}))^3}{q}\right]^{\text{Pi}} \quad (1)$$

where n is the number of structural levels observed, G is the Guinier prefactor, R_g is the radius of gyration and B is a prefactor specific to the type of power-law scattering which is specified as the decay of the exponent P .

Additionally, the presence of a correlation peak was observed in samples at 58% and 100% D_2O and was attributed to lysozyme domains. The correlation effect is incorporated into the general scattering intensity description as follows:^[27]

$$I(q) = \text{AF}(q)^2 S(q) \quad (2)$$

where $\text{AF}(q)^2$ is the scattered intensity for non-correlated domains and corresponds to Equation 1.^[27] $S(q)$ is the structure factor that, in the unified fit, accounts for weak correlations between the domains and was only applied to modify the protein structural level. All remaining structural levels were not affected by $S(q)$. In the unified fit method, a semi-empirical function based on Born-Green theory that describes the correlations between the domains given by

$$S(q) = \frac{1}{1 + k\Theta} \quad (3)$$

and

$$\Theta = 3 \frac{\sin(q\zeta) - q\zeta \cos(q\zeta)}{(q\zeta)^3} \quad (4)$$

where k is the degree of correlation and ζ is the averaged distance between the correlated domains.^[27]

The maximum entropy (MaxEnt) size distribution method^[39–41] also available in Irena routine^[36] was used to measure the polydispersity of the silica particles. By using the MaxEnt method a histogram is obtained which corresponds to the maximum configurational entropy compatible with the data. This approach has been successfully applied to determine the size distribution in a wide range of different materials.^[41–45]

Supporting Information

Supporting Information is available from the Wiley Online Library or from the author.

Acknowledgements

The authors acknowledge Dr. Tammy Metroke (Universal Technology Corporation at the Air Force Research Laboratory, Tyndall AFB, FL) for assistance with adsorption/desorption isotherms and BET measurements and to Karen Kelley (University of Florida, Gainesville, Florida) for SEM and TEM images provided as a service through ICBR Electron Microscopy Biolmaging Lab. The Air Force Research Laboratory (AFRL) work was supported by the funding from the AFRL-Materials and Manufacturing directorate and the Defense Threat Reduction Agency-Joint Science and Technology Office (Project Code AA06CBT008 (Jennifer Becker, Ilya Elashvili, and Stephen Lee, Program Managers)). Research at Oak Ridge National Laboratory (ORNL) was sponsored by the Laboratory Directed Research and Development Program of ORNL. The authors also acknowledge support from ORNL's Center for Structural Molecular Biology (CSMB) that is supported by the Office of Biological and Environmental Research, U. S. Department of Energy. This manuscript has been coauthored by UT-Battelle, LLC, under Contract No. DE-AC05-00OR22725 with the U.S. Department of Energy. M.B.C. thanks Capes-Brazil for research support.

Received: June 7, 2010
Published online: July 9, 2010

- [1] N. Kröger, R. Deutzmann, M. Sumper, *Science* **1999**, *286*, 1129.
- [2] H. A. Currie, C. C. Perry, *Ann. Bot.* **2007**, *100*, 1383.
- [3] R. R. Naik, L. L. Brott, S. J. Clarson, M. O. Stone, *J. Nanosci. Nanotechnol.* **2002**, *2*, 95.
- [4] N. Kröger, R. Deutzmann, M. Sumper, *J. Biol. Chem.* **2001**, *276*, 26066.
- [5] K. Shimizu, J. Cha, G. D. Stucky, D. E. Morse, *Proc. Natl. Acad. Sci. USA* **1998**, *95*, 6234.
- [6] J. N. Cha, K. Shimizu, Y. Zhou, S. C. Christiansen, B. F. Chmelka, G. D. Stucky, D. E. Morse, *Proc. Natl. Acad. Sci. USA* **1999**, *96*, 361.
- [7] D. Ivnitski, K. Artyushkova, R. A. Rincon, P. Atanassov, H. R. Luckarift, G. R. Johnson, *Small* **2008**, *4*, 357.
- [8] D. Belton, S. V. Patwardhan, C. C. Perry, *J. Mater. Chem.* **2005**, *15*, 4629.
- [9] K. M. Roth, Y. Zhou, W. Yang, D. E. Morse, *J. Am. Chem. Soc.* **2005**, *127*, 325.
- [10] N. Kröger, *Curr. Opin. Chem. Biol.* **2007**, *11*, 662.
- [11] C. C. Perry, D. Belton, K. Shafran, *Prog. Mol. Subcell. Biol.* **2003**, *33*, 269.
- [12] L. Betancor, H. R. Luckarift, *Trends Biotechnol.* **2008**, *26*, 566.
- [13] H. R. Luckarift, J. C. Spain, R. R. Naik, M. O. Stone, *Nat. Biotechnol.* **2004**, *22*, 211.
- [14] V. Pipich, M. Balz, S. E. Wolf, W. Tremel, D. Schwahn, *J. Am. Chem. Soc.* **2008**, *130*, 6879.
- [15] O. Vidal, M. C. Robert, F. Boue, *J. Cryst. Growth* **1998**, *192*, 271.
- [16] S. C. Teixeira, J. Ankner, M. C. Bellissent-Funel, R. Bewley, M. P. Blakeley, L. Coates, R. Dahint, R. Dalgliesh, N. Dencher, J. Dhont, P. Fischer, V. T. Forsyth, G. Fragneto, B. Frick, T. Geue, R. Gilles, T. Gutberlet, M. Haertlein, T. Hauss, W. Haussler, W. T. Heller, K. Herwig, O. Holderer, F. Juranyi, R. Kampmann, R. Knott, J. Kohlbrecher, S. Kreuger, P. Langan, R. Lechner, G. Lynn, C. Majkrzak, R. May, F. Meilleur, Y. Mo, K. Mortensen, D. A. Myles, F. Natali, C. Neylon, N. Niimura, J. Ollivier, A. Ostermann, J. Peters, J. Pieper, A. Ruhm, D. Schwahn, K. Shibata, A. K. Soper, T. Straessle, U. I. Suzuki, I. Tanaka, M. Tehei, P. Timmins, N. Torikai, T. Unruh, V. Urban, R. Vavrin, K. Weiss, G. Zaccai, *Chem. Phys.* **2008**, *345*, 133.
- [17] C. Neylon, *Eur. Biophys. J.* **2008**, *37*, 531.
- [18] G. M. Luo, Q. Zhang, A. R. Del Castillo, V. Urban, H. O'Neill, *ACS Appl. Mater. Interfaces* **2009**, *1*, 2262.
- [19] K. S. W. Sing, D. H. Everett, R. A. W. Haul, L. Moscou, R. A. Pierotti, J. Rouquerol, T. Siemieniowska, *Pure Appl. Chem.* **1985**, *57*, 603.

- [20] C. C. F. Blake, D. F. Koenig, G. A. Mair, A. C. T. North, D. C. Phillips, V. R. Sarma, *Nature* **1965**, 206, 757.
- [21] H. R. Luckarift, M. B. Dickerson, K. H. Sandhage, J. C. Spain, *Small* **2006**, 2, 640.
- [22] I. Schmidt, F. Cousin, C. Huchon, F. Boue, M. A. V. Axelos, *Biomacromolecules* **2009**, 10, 1346.
- [23] J. Gummel, F. Boue, B. Deme, F. Cousin, *J. Phys. Chem. B* **2006**, 110, 24837.
- [24] J. Gummel, F. Cousin, F. Boue, *Macromolecules* **2008**, 41, 2898.
- [25] F. Cousin, J. Gummel, D. Ung, F. Boue, *Langmuir* **2005**, 21, 9675.
- [26] N. Stribeck, *X-Ray Scattering of Soft Matter*, Springer, **2007**.
- [27] G. Beaucage, T. A. Ulibarri, E. P. Black, D. W. Schaefer, in *Hybrid organic-inorganic composites*, Vol. 1 (Eds: J. E. Mark, C. Y.-C. Lee, P. A. Bianconi), **1995**, 97.
- [28] M. A. da Silva, R. Itri, E. P. G. Areas, *Biophys. Chem.* **2002**, 99, 169.
- [29] C. J. Brinker, G. W. Scherer, *Sol-Gel Science: The Physics and Chemistry of Sol-Gel Processing*, Academic Press, **1990**.
- [30] K. D. Keefer, in *Silicon-Based Polymer Science: A Comprehensive Resource*, (Eds: J. M. Zeigler, F. W. Fearon), Oxford University Press, **1989**, 227.
- [31] L. C. Klein, *Annu. Rev. Mater. Sci.* **1985**, 15, 227.
- [32] M. Vallet-Regi, "Ordered mesoporous materials in the context of drug delivery systems and bone tissue engineering", presented at *1st European Chemistry Congress*, Budapest, HUNGARY, Aug 27–31, **2006**.
- [33] T. Shiomi, T. Tsunoda, A. Kawai, F. Mizukami, K. Sakaguchi, *Chem. Mater.* **2007**, 19, 4486.
- [34] Assumes a spherical shape for lysozyme with radius 1.7×10^{-9} nm. The surface covered by one molecule is 9×10^{-18} m². The surface covered by 9 mg is $((9 \times 10^{-3}) \times (9 \times 10^{-18} \text{ m}^2) \times (6.023 \times 10^{23}))/14300$.
- [35] G. W. Lynn, W. Heller, V. Urban, G. D. Wignall, K. Weiss, D. A. A. Myles, *Phys. B Cond. Mat.* **2006**, 385–386, 880.
- [36] J. Ilavsky, P. R. Jemian, *J. Appl. Crystallogr.* **2009**, 42, 347.
- [37] G. Beaucage, *J. Appl. Crystallogr.* **1995**, 28, 717.
- [38] G. Beaucage, *J. Appl. Crystallogr.* **1996**, 29, 134.
- [39] J. A. Potton, G. J. Daniell, B. D. Rainford, *J. Appl. Crystallogr.* **1988**, 21, 663.
- [40] J. A. Potton, G. J. Daniell, B. D. Rainford, *J. Appl. Crystallogr.* **1988**, 21, 891.
- [41] P. R. Jemian, J. R. Weertman, G. G. Long, R. D. Spal, *Acta Metall. Mater.* **1991**, 39, 2477.
- [42] L. L. Araujo, R. Giulian, D. J. Sprouster, C. S. Schnohr, D. J. Llewellyn, P. Kluth, D. J. Cookson, G. J. Foran, M. C. Ridgway, *Phys. Rev. B* **2008**, 78.
- [43] Y. P. Li, W. G. Chi, S. Sampath, A. Goland, H. Herman, A. J. Allen, J. Ilavsky, *J. Am. Cer. Soc.* **2009**, 92, 491.
- [44] A. J. Allen, J. J. Thomas, H. M. Jennings, *Nat. Mater.* **2007**, 6, 311.
- [45] M. K. Ridley, V. A. Hackley, M. L. Machesky, *Langmuir* **2006**, 22, 10972.